Design and optimized control of a 6-ups vibration platform for low-frequency whole-vehicle testing

Huakui Chen[1], Xuan Jia[2], Shuai Zhang[3], Yuqing Xi[4], Kui Liu[5], Yuzhuo Zhang[6]
[1]School of Automotive and Rail Transit, Luoyang Polytechnic, Luoyang, 471000, China
[2, 3, 6]School of Vehicle and Traffic Engineering, Henan University of Science and Technology, Luoyang, 471003, China
[4]Luoyang Vocational College of Science and Technology, Luoyang, 471822, China
[2, 3]State Key Laboratory of Intelligent Agricultural Power Equipment, Luoyang, 471003, China
[5]China YITUO Group Co., Ltd., Luoyang 471003, China
[3]Corresponding author
E-mail: [1]*huakuichen2022@163.com*, [2]*g13733898511@163.com*, [3]*boreke@126.com*, [4]*yuqingxi2022@163.com*, [5]*liukuijy@163.com*, [6]*yuzhuozhang@haust.edu.cn*

Received 6 May 2026; accepted 8 October 2026; published online 24 November 2026
DOI https://doi.org/10.21595/jve.2026.26650

Check for updates

Copyright © 2026 Huakui Chen, et al. This is an open access article distributed under the Creative Commons Attribution License, which permits unrestricted use, distribution, and reproduction in any medium, provided the original work is properly cited.

Abstract. This study designs a 6-UPS platform for low-frequency whole-vehicle and chassis-assembly vibration tests in the 0.1-25 Hz band. Kinematic and dynamic models establish the relationship between the moving platform and the six electric cylinders. Horizontal Hooke joints, spherical joints, and a servo electric-cylinder drive are selected, and static and modal analyses evaluate structural performance. A hybrid particle-swarm and tabu-variable-neighborhood algorithm is used to tune the PID controller. Compared with Ziegler-Nichols tuning in the reported simulations, overshoot decreases by 75.86 %, settling time by 29.41 %, and maximum spatial displacement error by approximately 61 %. Simulations also reproduce the target vertical displacement histories for a synthetic Class E road and a measured tractor rotary-tillage condition. Quantitative road-spectrum reproduction errors remain to be calculated from the paired time-history data. The results provide a design and simulation basis for subsequent prototype testing.

Keywords: design, optimized control,6-UPS vibration platform, low-frequency whole-vehicle testing, road spectrum reproduction.

1. Introduction

Vehicle vibration tests are used to assess ride comfort and component durability [1-4]. Six-degree-of-freedom parallel mechanisms provide a stiff structure and load-bearing capacity for multi-axis excitation [5-9]. This study designs a 6-UPS vibration platform with horizontal Hooke joints and spherical joints and evaluates a hybrid heuristic algorithm for PID tuning.

This study targets the low-frequency vibration test requirements of whole vehicles and key chassis assemblies (e.g., suspension systems and powertrain mounts), with a core focus on road spectrum reproduction and ride comfort verification. Unlike high-frequency component vibration test benches (usually covering up to 2000 Hz for electronic components and small parts), the designed 6-UPS platform is oriented to whole-vehicle and large-scale assembly tests, with a designed working frequency band of 0.1–25 Hz. This frequency range covers the main vibration energy interval of vehicle road excitation, body rigid modal vibration, and chassis system dynamic response.

Correspondingly, the core design requirements are determined as follows:

1. Load capacity: Rated load of 1200 kg, to meet the test needs of light vehicles and large agricultural machinery chassis;

2. Motion stroke: ±150 mm translational stroke and ±10° deflection angle, to reproduce large-displacement vibration input of real road surfaces;

3. Motion accuracy: Displacement control error within 0.1 mm, to ensure the fidelity of road

spectrum reproduction;

4. Structural reliability: Avoid resonance within the working frequency band and ensure sufficient stiffness and strength under rated load.

The 6-UPS parallel mechanism is selected for this scenario because it has significant advantages over series mechanisms in bearing capacity, motion accuracy and structural stiffness, and can realize six-degree-of-freedom coupled vibration input which cannot be achieved by single-axis vibration shakers. The horizontal Hooke hinge is adopted instead of the conventional cross-axis Hooke hinge to solve the problem of stiffness attenuation and poor stability under heavy load and large swing angle conditions, which is more suitable for heavy-load low-frequency vibration test scenarios.

Vehicle vibration platforms reproduce driving excitations for components and complete vehicles [10, 11]. Platforms with limited degrees of freedom cannot reproduce all six components of vehicle motion [12-15]. Serial mechanisms may also accumulate positioning errors and have limited load capacity [16, 17]. Stewart-type parallel mechanisms offer high structural stiffness, positioning accuracy, and load-bearing capacity [18-20]. This study therefore examines a six-degree-of-freedom parallel platform, its connecting joints, and its control strategy.

Research on six-degree-of-freedom platforms has addressed vibration isolation, workspace, positioning accuracy, and motion control. Zheng et al. [21] developed a quasi-zero-stiffness isolator. Song et al. [22] optimized a 6-UPS mechanism with the Taguchi method and entropy-weighted grey relational analysis. Liu et al. [23] studied its workspace, while Zhang et al. [24] investigated motion measurement. Other work has examined forward-kinematics solutions [25], spherical-wheel motion platforms [26], and dynamic modeling [27]. These studies motivate further examination of joint design, PID tuning, and road-spectrum reproduction for a low-frequency heavy-load platform.

In this paper, a 6-UPS vehicle vibration test platform based on horizontal universal joints and spherical joints was designed, the kinematic/dynamic modeling and structural performance verification were completed, a PID control strategy optimized by a hybrid heuristic algorithm was proposed, and finally the platform performance verification was accomplished through the reproduction of actually collected road spectra.

The platform is mainly used to study vibration fatigue failure of chassis structural parts, attenuation performance of suspension vibration isolation systems, and ride comfort response of the whole vehicle under road excitation. It is applicable to test articles with a base size within 1.2 m×1.2 m and a weight within 1200 kg.

2. Platform design and control optimization research methods

The methods and processes used in the vehicle six-freedom test platform design and control optimization research are shown in Fig. 1.

This study focuses on the design and control optimization of a 6-UPS vibration test platform, and sequentially carries out four core tasks: kinematic and dynamic modeling of the mechanism, design and performance verification of key structures, optimization and simulation verification of control strategies, and real-vehicle road spectrum reproduction tests. Detailed research contents and results are presented in subsequent chapters.

3. Vehicle vibration test platform modeling

3.1. Kinematics modeling and analysis

The six-degree-of-freedom vehicle vibration test platform has four key components: a moving platform, a fixed platform, driving branches and joint hinges. The two platforms are connected in parallel via hinges using driving branches. With the telescopic motion of six driving branches, the moving platform can achieve six degrees of freedom in space and simulate various spatial

postures. In the figure, L_1-L_6, A_1-A_6, and B_1-B_6 represent the positions of the six driving branches, upper hinge points, and lower hinge points respectively. Through the coordinated movement of six drive branches, the moving platform can achieve specified movements. After the coordinate system is established, the platform's posture is represented by the generalized coordinate vector $\mathbf{q} = [q_t \quad q_r]$, where q_t and q_r represent the position vector and attitude angle of the moving platform center in the inertial coordinate system. Assuming the coordinate vectors of the conjoined coordinate system {**A**} and the inertial coordinate system {**B**} are parallel but their origins don't coincide, there is a translation transformation relationship between them. Translate the inertial coordinate system O_b-$X_bY_bZ_b$ along the XYZ axis to make O_b coincide with O_a, obtaining the translation transformation matrix **T**:

$$T = [xyz]^T. \tag{1}$$

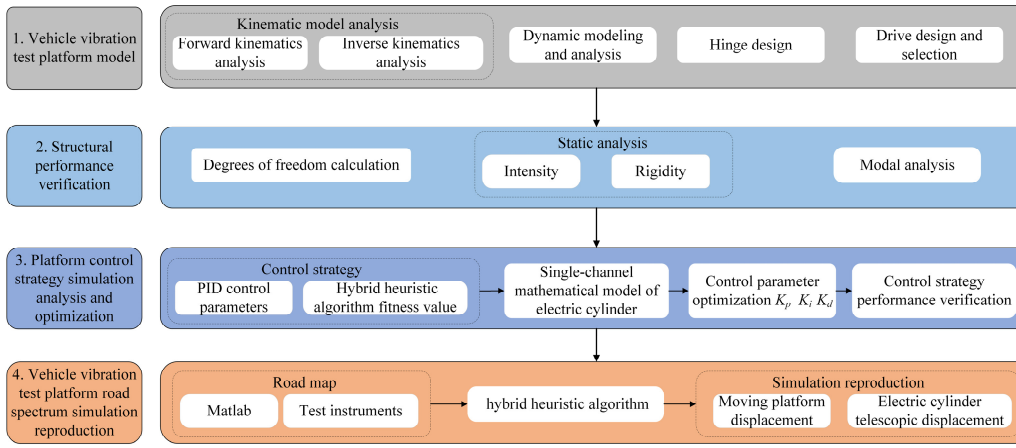

Fig. 1. Six-freedom test platform design and control optimization research process

Assuming that the coordinate origins of the conjoined coordinate system {**A**} and the inertial coordinate system {**B**} are the same, but their coordinate vectors are not parallel, it is said that there is a rotation transformation relationship between the two coordinate systems. Rotate the inertial coordinate system O_b-$X_bY_bZ_b$ in sequence along the XYZ axis so that the coordinate system completely coincides with the coordinate axis of the conjoined coordinate system, thereby obtaining the rotation transformation matrix.

After three rotation transformations, the obtained rotation transformation matrix **R** is:

$$R = \begin{bmatrix} \cos\gamma\cos\beta & \cos\gamma\sin\beta\sin\alpha - \sin\gamma\cos\alpha & \sin\gamma\sin\alpha + \cos\alpha\cos\gamma\sin\beta \\ \sin\gamma\cos\beta & \cos\gamma\cos\alpha - \sin\alpha\sin\gamma\sin\beta & \sin\gamma\sin\beta\cos\alpha - \cos\gamma\sin\alpha \\ -\sin\beta & \cos\beta\sin\alpha & \cos\beta\cos\alpha \end{bmatrix}. \tag{2}$$

However, in most cases, the coordinate origins and coordinate vectors of the conjoined coordinate system {**A**} and the inertial coordinate system {**B**} are different. Therefore, the homogeneous transformation matrix **Q** can be used to comprehensively represent its translation and rotation transformation:

$$\mathbf{Q} = \begin{bmatrix} \mathbf{R} & \mathbf{T} \\ 0 & 1 \end{bmatrix}, \tag{3}$$

where **R** is the rotation matrix; **T** is the position vector.

Combining Eq. (1) with Eq. (3), we can get the transformation matrix Q from the inertial coordinate system O_b-$X_bY_bZ_b$ to the conjoined coordinate system O_a-$X_aY_aZ_a$:

$$\mathbf{Q}=\begin{bmatrix}\cos\gamma\cos\beta & \cos\gamma\sin\beta\sin\alpha-\sin\gamma\cos\alpha & \sin\gamma\sin\alpha+\cos\alpha\cos\gamma\sin\beta & x\\ \sin\gamma\cos\beta & \cos\gamma\cos\alpha-\sin\alpha\sin\gamma\sin\beta & \sin\gamma\sin\beta\cos\alpha-\cos\gamma\sin\alpha & y\\ -\sin\beta & \cos\beta\sin\alpha & \cos\beta\cos\alpha & z\\ 0 & 0 & 0 & 1\end{bmatrix}. \tag{4}$$

3.1.1. Kinematics back solution analysis

If the spatial position and attitude of the moving platform of the vehicle vibration test platform are known, solving the displacements of the six driving branches is called the inverse position solution. When the radius R_a of the moving platform and the radius R_b of the fixed platform are known, the length vector $\mathbf{L}_i$ of the driving branch chain can be expressed as:

$$\mathbf{L}_i=\mathbf{R}\mathbf{A}_i+\mathbf{E}_i-\mathbf{B}_i,\quad (i=1,2,\ldots,6), \tag{5}$$

where $\mathbf{R}$ is the rotation transformation matrix; $\mathbf{A}_i$ is the position vector at the joint of the moving platform and the upper hinge; $\mathbf{B}_i$ is the position vector at the junction of the fixed platform and the lower hinge; $\mathbf{E}_i$ is the unit matrix.

It can be seen from the definition of vector module that the length l_i of the i-th driving branch is:

$$l_i=\sqrt{\mathbf{L}_i^T\mathbf{L}_i},\quad (i=1,2,\ldots,6). \tag{6}$$

The displacement S_i of the driving branch is:

$$S_i=l_i-l_0,\quad (i=1,2,\ldots,6), \tag{7}$$

where l_0 represents the initial length of the driving branch chain.

Differentiating the rod length formula yields the velocity and acceleration mapping relationship between the actuated limbs and the moving platform, laying a foundation for subsequent dynamic modeling and control.

3.1.2. Forward kinematics analysis

If the displacement of the six driving branches in the vehicle vibration test platform is known, solving the spatial position and attitude of the moving platform is the positive position solution. The forward kinematics problem is complex, and current solution methods mainly include analytical, sensor and numerical iteration methods. Considering engineering practice, the numerical iteration method is efficient and can provide real-time, stable and accurate solutions. So, this paper uses the numerical iteration method to analyze the forward position of the vehicle vibration test platform. Let $\boldsymbol{\varphi}_i$ represent the unit vector of the i-th driving branch, then:

$$\mathbf{p}+\mathbf{q}_i-\mathbf{b}_i=l_i\boldsymbol{\varphi}_i,\quad (i=1,2,\ldots,6), \tag{8}$$

where $\mathbf{p}$ is the position vector of the center of the moving platform in the inertial coordinate system; $\mathbf{p}_i$ is the position vector of the upper hinge coordinate point; $\mathbf{b}_i$ is the position vector of the lower hinge coordinate point; $\mathbf{q}_i=\mathbf{R}\mathbf{p}_i$; $\boldsymbol{\varphi}_i=\mathbf{L}_i/\|\mathbf{L}_i\|$.

It can be known from the knowledge of robot kinematics:

$$\dot{\mathbf{q}}_i=\frac{d}{dt}(\mathbf{R}\mathbf{p}_i)=\dot{\mathbf{R}}\mathbf{p}_i=\boldsymbol{\omega}\times\mathbf{q}_i,\quad (i=1,2,\ldots,6), \tag{9}$$

where $\boldsymbol{\omega}$ stands for the angular speed of the moving platform circling around the inertial

coordinate system. Since position vectors $\mathbf{A}_i$ and $\mathbf{B}_i$ remain unchanged in their respective coordinate systems, therefore:

$$\dot{\mathbf{b}}_i = 0, \quad \dot{\mathbf{p}}_i = 0, \quad (i = 1,2,\ldots,6). \tag{10}$$

Combining Eq. (8-10) yields:

$$i_i\boldsymbol{\varphi}_i + l_i\dot{\boldsymbol{\varphi}}_i = \dot{\mathbf{p}} + \boldsymbol{\omega} \times \mathbf{q}_i, \quad (i = 1,2,\ldots,6). \tag{11}$$

Knowing ${\varphi_i}^T\varphi_i = 1$ and ${\varphi_i}^T\varphi_i = 0$, multiply both sides of the equal sign in Eq. (11) by $\boldsymbol{\varphi}_i^T$ at the same time to get:

$$\dot{l}_i = \boldsymbol{\varphi}_i^T\dot{\mathbf{p}} + (\mathbf{q}_i \times \boldsymbol{\varphi}_i)^T\boldsymbol{\omega} = [\boldsymbol{\varphi}_i^T \quad (\mathbf{q}_i \times \boldsymbol{\varphi}_i)^T]\begin{bmatrix}\dot{\mathbf{p}}\\ \boldsymbol{\omega}\end{bmatrix}, \quad (i = 1,2,\ldots,6). \tag{12}$$

According to the definition of the Jacobian matrix, the relationship between the velocity vector of the driving branch in the vehicle vibration test platform and the generalized velocity vector of the moving platform is:

$$\dot{\mathbf{E}} = J\dot{\mathbf{R}}. \tag{13}$$

Therefore, the Jacobian matrix **J** of the vehicle vibration test platform is:

$$\mathbf{J} = \begin{bmatrix}\boldsymbol{\varphi}_1 & \boldsymbol{\varphi}_2 & \cdots & \boldsymbol{\varphi}_6\\ \mathbf{q}_1 \times \boldsymbol{\varphi}_1 & \mathbf{q}_2 \times \boldsymbol{\varphi}_2 & \cdots & \mathbf{q}_6 \times \boldsymbol{\varphi}_6\end{bmatrix}^T. \tag{14}$$

It is explained that the forward kinematics solution of the 6-UPS mechanism is difficult to solve. Combined with engineering practice, this paper adopts the numerical iteration method to complete the forward kinematics solution.

The Newton iteration can be obtained as:

$$P^{k+1} = P^k - J_k^{-1}f(P^k) = P^k - J_k^{-1}f(L_k - L_d). \tag{15}$$

In summary, the correct solution problem of the vehicle vibration test platform is transformed into an optimization problem. By calculating the Jacobian matrix, the iterative formula shown in Eq. (15) is constructed. When $L_k = L$, $\|L_k - L_d\| = 0$, at this time $F(P)$ obtains the optimal value. In engineering practice, the absolute accuracy $\|L_k - L_d\| \leq \varepsilon$ is taken as the iteration termination condition, and the optimal solution P^k obtained at this time is the positive solution result.

3.2. Dynamic modeling and analysis

The Lagrange method uses the energy of the system to establish dynamic equations. The Lagrange function of the vehicle vibration test platform can be expressed as:

$$E = E_k - E_p, \tag{16}$$

where E_k represents the total kinetic energy of the system; E_p represents the total potential energy of the system.

The inertial coordinate system O_b-$X_bY_bZ_b$ on the fixed platform of the vehicle vibration test platform is selected as the reference coordinate system for the kinetic energy and potential energy of the system. Since the driving branches of the vehicle vibration test platform are all composed of rigid rods, the generalized coordinate of its posture is $\mathbf{q} = [q_t \quad q_r]$, so the Lagrange equation of the test platform can be expressed as:

$$\frac{d}{dt}\left(\frac{\partial L(\mathbf{q},\dot{q})}{\partial \dot{q}}\right)-\frac{\partial L(\mathbf{q},\dot{q})}{\partial \mathbf{q}}=\mathbf{F}, \tag{17}$$

where $\mathbf{F}$ is the generalized force on the generalized coordinate $\mathbf{q}$ of the moving platform. When solving the system kinetic and potential energy of the vehicle vibration test platform, the test platform is divided into two subsystems: the parallel mechanism dynamic platform and the parallel mechanism drive branch chain. The system is simplified as follows: (1) Treat the upper hinge and moving platform as one part; (2) Treat the lower hinge and drive branch as one part; (3) Treat the drive branch as a simple two - force rod; (4) Ignore the rotation around its own axis between the telescopic rods of the driving branch chain; (5) Ignore the friction and clearance between the moving pairs.

Assume that the posture change of the moving platform is $\mathbf{q}=[x \quad y \quad z \quad \alpha \quad \beta \quad \gamma]^T$, then the translation speed v_p and rotation speed ω_p of the moving platform are $\mathbf{v}_p=[\dot{x} \quad \dot{y} \quad \dot{z}]^T$ and $\boldsymbol{\omega}_p=[\dot{\alpha} \quad \dot{\beta} \quad \dot{\gamma}]^T$ respectively.

Through the calculation of the system's kinetic and potential energy, the Lagrangian dynamic equation of the platform was finally established. Given the system kinetic energy and potential energy of the vehicle vibration test platform, the Lagrange dynamics equation of the vehicle vibration test platform established by Eq. (18) is:

$$\mathbf{F}=\frac{d}{dt}\left(\frac{\partial\left(E_{kp}+E_{kl}\right)}{\partial \dot{\mathbf{q}}}\right)-\frac{\partial\left(E_{kp}+E_{kl}\right)}{\partial \mathbf{q}}-\frac{\partial\left(E_{pp}+E_{pl}\right)}{\partial \mathbf{q}}. \tag{18}$$

Rewriting Eq. (18) into vector form can be expressed as:

$$F=M(\mathbf{q})\ddot{\mathbf{q}}+V(\mathbf{q},\dot{\mathbf{q}})\dot{\mathbf{q}}+\mathbf{G}(\mathbf{q}), \tag{19}$$

where $\mathbf{M}(q)$ is the mass inertia matrix of the vehicle vibration test platform; $\mathbf{V}(q)$ is the Coriolis force and centrifugal force vector matrix of the vehicle vibration test platform; $\mathbf{G}(q)$ is the gravity vector matrix of the vehicle vibration test platform.

3.3. Structural design and parameter selection

The expected performance indicators of the vehicle vibration test platform are proposed based on the general frequency and acceleration laws of vibration tests of vehicles and their system components. They are suitable for vibration testing of the entire vehicle and its system components. Its expected performance indicators are shown in Table 1.

3.3.1. Hinge design

For automotive vibration testing, random vibration and road spectrum replication are the most widely used test methods, while sine sweep testing is a basic means for platform system identification and modal calibration. The designed platform supports all the above test modes, and this paper focuses on the verification of road spectrum replication capability, which is the core demand of vehicle whole-machine testing.

Conventional cross-axis Hooke's hinges are widely used in light-load precision parallel mechanisms, but for heavy-load vehicle vibration test platforms with large swing angles, they have obvious defects: the stiffness of the hinge pair decreases significantly with the increase of swing angle in the working space, and the force condition of the cross-axis deteriorates under heavy load, leading to insufficient operational stability and aggravated wear.

The proposed horizontal Hooke joint is intended to improve load transmission at large swing angles. A spherical joint is paired with it to accommodate motion of the six branches. The rated-load analysis in Section 4.2 evaluates the overall structure; a separate contact-stress and wear

assessment of the joints remains necessary.

Table 1. Expected performance index

Performance index	Title 2
Degrees of freedom	6
Platform size $r \times R$	600 mm×850 mm
Bearing capacity	1200 kg
Maximum translation amount	±150 mm
Maximum deflection	±10°
Working frequency	0.1-25 Hz
Basic test waveforms	Sine wave, random vibration, time history replication
Note: Sine wave is used as the basic calibration waveform for platform dynamic performance testing and system parameter identification. In practical vehicle test applications, the platform supports random vibration tests and measured road spectrum time history replication, as verified in Section 6	

3.3.2. Drive design and selection

According to the platform's rated load capacity of 1200 kg, the calculated rated thrust of the drive unit is no less than 11.76 kN. The final selected model is the DDA80 series servo electric cylinder with the matching ECMA-FX1315FS servo motor.

3.3.3. System configuration and structural parameter design

Considering the comprehensive bearing characteristics and overall performance, this paper selects the 6-UPS parallel mechanism as the main configuration of the platform and clarifies the kinematic pair types corresponding to U, P, and S.

According to the literature [22], when $r = 500$ mm, $R = 800$ mm, $\alpha = 85°$, $\beta = 30°$ and $H = 1100$ mm, the test platform has better comprehensive performance. Thus, these parameters are chosen as the initial structural parameters, the designed vehicle vibration test platform is shown in Fig. 2.

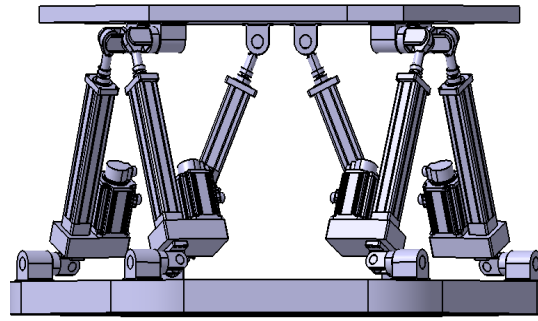

Fig. 2. Three-dimensional model of vehicle vibration test platform

Table 2. Parameter comparison with typical commercial 6-DOF vibration platforms

Parameter index	Typical electro-hydraulic 6-DOF platform	Typical electromagnetic 6-DOF platform	Proposed 6-UPS platform
Rated load	1000 – 1500 kg	100 – 300 kg	1200 kg
Z-axis stroke	±100 – ±150 mm	±10 – ±30 mm	±150 mm
Working frequency	0.1-50 Hz	5-2000 Hz	0.1-25 Hz
Drive mode	Electro-hydraulic actuator	Electromagnetic shaker	Servo electric cylinder
Typical application	Heavy-load motion simulation	High-frequency component test	Low-frequency whole-vehicle road spectrum test

Table 2 compares the design targets of the proposed platform with representative platform

categories. The proposed servo electric-cylinder configuration targets a 1200 kg load and a ±150 mm vertical stroke over 0.1-25 Hz; comparative performance claims require measurements under matched test conditions.

4. Vibration test platform structural performance analysis

4.1. Degrees of freedom calculation

Calculated separately using the structural degree-of-freedom formula and the Kutzbach-Grubler formula, the designed platform has 6 degrees of freedom, fully meeting the design requirements for six-degree-of-freedom motion.

4.2. Static analysis

The static analysis in this paper is carried out under the rated load of 1200 kg, which is the design working condition of the platform. The platform performance under different load levels will be further tested and analyzed in follow-up prototype tests.

Structural stiffness and strength affect displacement tracking and the load-bearing performance of the test platform. The static analysis therefore evaluates the rated-load condition while considering the structural mass.

A vertical load of 12,000 N, approximately corresponding to the rated load of 1200 kg, is applied in the static model. The results are shown in Fig. 3.

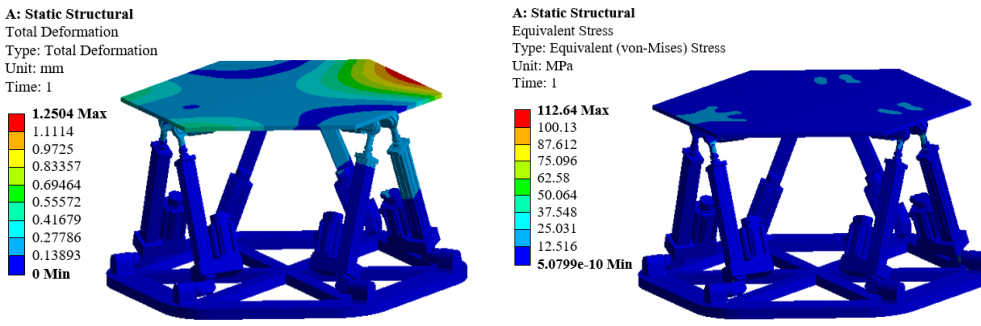

a) b)

Fig. 3. Static analysis of vehicle vibration test platform

Under the applied load, the predicted maximum deformation is 1.25 mm, mainly at the moving-platform edge. The maximum equivalent stress is 112.64 MPa at its spherical-joint connection. This value is below the nominal yield strength of Q235 steel (235 MPa) in the modeled condition. These results support the strength assessment of the overall model but do not establish the local contact stress or fatigue life of each joint.

The horizontal Hooke joints and spherical joints are represented in the whole-platform finite-element model, which predicts a maximum equivalent stress of 112.64 MPa at a spherical-joint connection. Because the joint interfaces are simplified, this result cannot be used as a component-level contact-stress or wear limit. A separate analysis of contact stress, fatigue, and wear at the joint interfaces is planned during prototype development, followed by experimental verification under rated load and large swing angles.

4.3. Modal performance analysis

The finite-element model used for the static analysis is transferred to the modal-analysis module, with the constraints adjusted for the modal calculation. Table 3 lists the first six reported elastic modes and their natural frequencies.

The first reported elastic natural frequency is 28.403 Hz, above the nominal upper working frequency of 25 Hz. The separation is approximately 3.403 Hz; excitation harmonics, load-dependent frequencies, damping, and the prototype boundary conditions should be assessed before claiming resonance avoidance over the full operating range.

Table 3. The first six natural frequencies and mode descriptions of the vehicle vibration test platform

Order	Frequency / Hz	Mode description	Mode type
1	28.403	First-order bending vibration of the moving platform along the X-axis	Elastic deformation mode
2	28.466	First-order bending vibration of the moving platform along the Y-axis	Elastic deformation mode
3	44.59	Torsional vibration of the moving platform around the Z-axis	Elastic deformation mode
4	69.852	Second-order bending vibration of the moving platform along the X-axis	Elastic deformation mode
5	69.938	Second-order bending vibration of the moving platform along the Y-axis	Elastic deformation mode
6	73.451	Vertical vibration of the moving platform with local hinge deformation	Elastic deformation mode

5. Platform control strategy design optimization and simulation verification

5.1. Control strategy based on hybrid heuristic algorithm

The hybrid heuristic algorithm combines particle swarm optimization (PSO) with tabu-variable-neighborhood search to tune the PID gains. Candidate gains are evaluated in Simulink using the dimensionless fitness function specified in Section 5.3.

PSO performs the global search, and tabu-variable-neighborhood search refines the candidate solution locally. The procedure is as follows:

1. Initialize the candidate PID gains K_p, K_i, and K_d within the prescribed actuator-model parameter ranges.

2. Evaluate the normalized overshoot, settling time, and steady-state error for each candidate using the Simulink model.

3. Apply PSO to identify a candidate solution through global search.

4. Refine the candidate with tabu-variable-neighborhood search while recording recently visited solutions.

5. Stop when the specified termination condition is met and report the selected PID gains.

The hybrid search is intended to combine global exploration with local refinement. Its performance relative to the Ziegler-Nichols method is compared in Section 5.3.

5.2. Single-channel mathematical model of electric cylinder

The servo electric cylinder, an independent system of a servo motor and a screw, converts the servo motor's rotational motion into the screw's linear motion. Also, it converts the servo motor's speed, revolution and torque control into the screw's speed, position and thrust control respectively. As the six branches of the vibration test platform consist of six identical electric cylinders, only one electric cylinder system needs independent analysis and modeling to simplify the controller design.

The transfer function of the electric cylinder from the driving voltage U_a to the output force F_{ml} is:

$$\begin{cases} G(s) = \dfrac{F_{ml}(s)}{U_a(s)} = \dfrac{k_m k_L k_{FT}(J_L s + b_L)}{a_4 s^4 + a_3 s^3 + a_2 s^2 + a_1 s + a_0}, \\ a_4 = J_m J_L J_a, \\ a_3 = (R + k_i) J_m J_L + (J_L b_m + J_m b_L) L_a, \\ a_2 = (R + k_i)(J_L b_m + J_m b_L) + (J_m k_L + b_m b_L +) L_a + (L_a k_L + k_m C_e) J_L, \\ a_1 = (R + k_i)(k_L J_L + J_m k_L + b_m k_L) + (b_m + b_L) L_a k_L + k_m C_e b_L, \\ a_0 = (R + k_i)(b_m + b_L) k_L + k_m C_e k_L, \end{cases} \tag{20}$$

where, k_m is the motor torque coefficient, k_L the equivalent stiffness of the motor shaft and belt, k_{FT} the proportional coefficient between screw shaft driving torque and electric cylinder sliding rod driving force, J_L and b_L the moment of inertia of the screw and drive shaft, R the armature resistance, k_i the motor current feedback coefficient, J_m the moment of inertia of the motor armature and shaft, b_m the viscous damping coefficient of the motor shaft, L_a the armature inductance, and C_e the motor back electromotive force coefficient.

5.3. Control parameter optimization

First, a single - channel mathematical model of the electric cylinder is used to simulate and analyze the control strategy. The simulation system's parameter selection is based on the actual parameters of the servo electric cylinder selected when designing the 3D model in this paper to get more realistic simulation data.

The transfer function of the single-leg system is obtained. The optimal Hankel norm approximation algorithm is used to reduce the system's order, and the second - order model of the reduced system is obtained:

$$G(s) = \frac{-0.0369s + 74.8}{s^2 + 6.647s + 26.6}. \tag{21}$$

Overshoot σ, settling time t_s, and absolute steady-state displacement error e_{ss} have different units and scales. They are therefore normalized by fixed positive reference values before aggregation:

$$J = \omega_1 \frac{\sigma}{\sigma_{ref}} + \omega_2 \frac{t_s}{t_{ref}} + \omega_3 \frac{|e_{ss}|}{e_{ref}}, \tag{22}$$

where σ is percentage overshoot, t_s is settling time in seconds, and e_{ss} is the absolute steady-state displacement error in millimetres. The reference values are $\sigma_{ref} = 15.74$ % and $t_{ref} = 0.34$ s (the Ziegler-Nichols baseline values in Table 4), and $e_{ref} = 0.1$ mm (the specified displacement-accuracy target). The dimensionless weights are $\omega_1 = 0.5$, $\omega_2 = 0.3$, and $\omega_3 = 0.2$, with $\omega_1 + \omega_2 + \omega_3 = 1$. All reference values are held fixed for both controllers; minimizing J emphasizes overshoot while accounting for settling time and steady-state error. The simulation implementation and the results in Table 4 must be checked against this normalized objective.

The single-cylinder transfer function is used as the plant for PID tuning. The candidate gains are evaluated in the Simulink model using the objective defined above.

A MATLAB implementation of the hybrid search is used to tune the PID gains for the electric-cylinder model.

For comparison, the same model is tuned with the Ziegler-Nichols (Z-N) method.

In MATLAB/Simulink, step response analysis was performed on the PID parameters obtained by hybrid heuristic algorithm optimization and Z-N method respectively. The comparison of step response results is shown in Fig. 4.

The resulting PID gains and step-response measures are reported in Table 4.

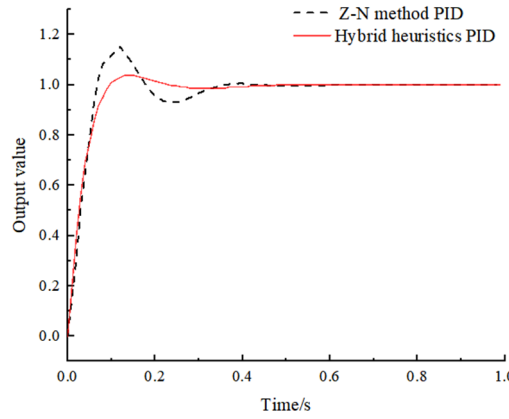

Fig. 4. Comparison of step response curves of the two control methods. The horizontal axis represents time in seconds, and the vertical axis represents normalized displacement output

Table 4. PID gains and step-response measures

Tuning method	K_p	K_i	K_d	Overshoot / %	Settling time / s
Ziegler–Nichols PID	64.4202	0.4564	1.3236	15.74	0.34
Hybrid heuristic PID	27.1923	1.7245	1.0636	3.80	0.24

Compared with Z-N tuning, the reported overshoot decreases from 15.74 % to 3.80 % (75.86 %) and the settling time from 0.34 s to 0.24 s (29.41 %). These are single-cylinder simulation results; the normalized-objective implementation must be confirmed before the comparison is attributed to the revised fitness function.

5.4. Control strategy performance verification

To verify the control performance of the hybrid heuristic algorithm PID, MATLAB/Simulink software is used to build a vehicle vibration test platform control simulation system controlled by this algorithm. The solution, physical component, and controller modules are encapsulated. A platform sensor module is added to the model to collect actual platform motion parameters. Using the built - in solution module in MATLAB/Simulink, motion inverse solution simulation is conducted, and the expansion and contraction variation of each electric cylinder is calculated according to the mobile platform's expected trajectory. To verify the control performance, the vibration test platform's simulation system model is simulated, and the error between the expected and actual positions of the moving platform is recorded via the sensor module. In the established simulation system, a composite motion trajectory is input, and the hybrid heuristic algorithm PID and Z-N method PID are used for control simulation of the control system model. The displacement of the upper platform's center point at maximum displacement during space movement is shown in Table 5.

Table 5. Comparison of displacement extremes of moving platform

Optimistic method	x-axis value		y-axis value		z-axis value	
	Max	Min	Max	Min	Max	Min
Z-N method	49.77	–49.84	25.21	–24.84	24.89	–24.86
Hybrid heuristic algorithm	50.09	–50.06	25.03	–25.08	24.95	–24.92

When using the hybrid heuristic algorithm for PID system control, the platform's spatial position change curve is closer to the input signal. With Z-N method PID control, each electric cylinder's motion error is within ±0.3 mm, and the upper platform's maximum displacement error in space is 0.23 mm. When using the hybrid heuristic algorithm-based PID control, the system stabilizes after 0.3 s, each electric cylinder's motion error is within ±0.1 mm, and the upper

platform's maximum displacement error in space is 0.09 mm. Moreover, the system's motion accuracy is enhanced by 61 %.

The controller is evaluated for the platform's 0.1-25 Hz design band. The sampling period, actuator bandwidth, and tracking accuracy under the full rated load require verification on the prototype.

The simulated cylinder tracking error is within ±0.1 mm for the reported test trajectory. Its extension to full-load and multi-axis road-spectrum tests requires experimental confirmation.

6. Vehicle vibration test platform road spectrum simulation verification

To validate the 6 - UPS vibration test platform's operational performance, tractor operating conditions are taken as an example. The tractor road spectrum is collected to control the electric cylinder for simulating and reproducing the road spectrum, verifying the designed six-degree-of-freedom vibration test system platform's performance.

6.1. Vehicle road spectrum data collection and analysis

A synthetic Class E road displacement history and a measured tractor rotary-tillage signal are selected as two verification conditions. These cases represent, respectively, a simulated rough-road input and a measured agricultural operating condition. Other road grades and loaded prototype conditions remain for future validation.

The test instruments for road spectrum signal collection include dynamic signal collectors, three - way acceleration sensors, Bluetooth communication interfaces, and computers with host computers. The test object is a high-horsepower wheeled tractor. The signal acquisition test frequency bandwidth is 0-512 Hz, frequency resolution is 0.5 Hz, and the average number is 50 times.

According to the experimental plan, multiple sets of effective data were collected for the tractor's set working conditions. After collection, the original signals need processing to support road spectrum simulation and reproduction. The signal at the acceleration sensor under rotary tillage conditions is selected for extraction and analysis.

Since abnormal impacts may occur during road spectrum signal collection, the collected acceleration signals have singular values that affect iteration accuracy and experiment reproducibility, so they need to be eliminated.

The road spectrum acquisition test is carried out on a wheeled tractor, with the scheme as follows:

1. Sensor arrangement: A three-way acceleration sensor is arranged at the connection between the tractor rear axle and the frame, which is the main vibration transmission position from the wheel to the vehicle body; the sensor is installed vertically along the Z-axis to collect vertical vibration acceleration signals;

2. Test parameters: The sampling frequency is set to 512 Hz, the frequency resolution is 0.5 Hz, and 50 groups of data are collected for average processing to eliminate random interference;

3. Data preprocessing: Singular value elimination and trend term removal are performed on the collected acceleration signals, and displacement time history signals are obtained through quadratic integration for subsequent vibration table reproduction.

6.2. Road spectrum reproduction of vehicle vibration test platform

A Class E road displacement history is simulated by harmonic superposition at $v = 10$ m/s. The measured tractor rotary-tillage acceleration history is preprocessed and integrated twice to obtain a displacement target. Fig. 5 shows the two target histories.

Each target road-spectrum history is applied as a vertical displacement command at the

moving-platform center. The target pose is converted into electric-cylinder commands using inverse kinematics. Fig. 6 shows the simulated vertical response under the hybrid-controller gains for the two conditions.

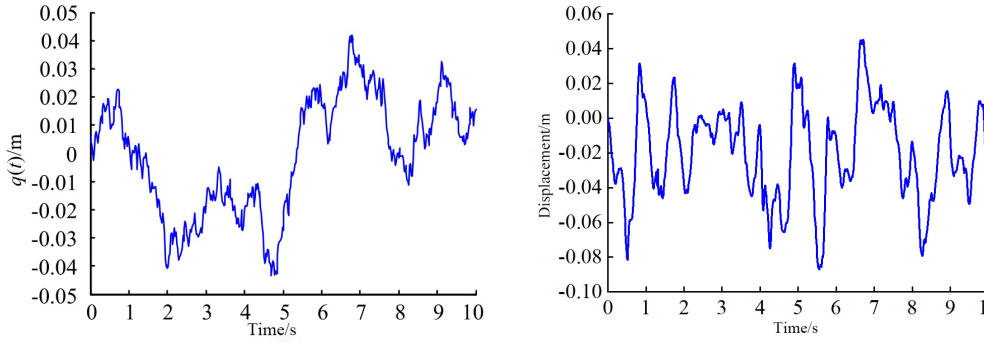

a) b)

Fig. 5. Simulation data of road spectrum signals: a) harmonic superposition method analog signal; b) actual vehicle working conditions collection signal

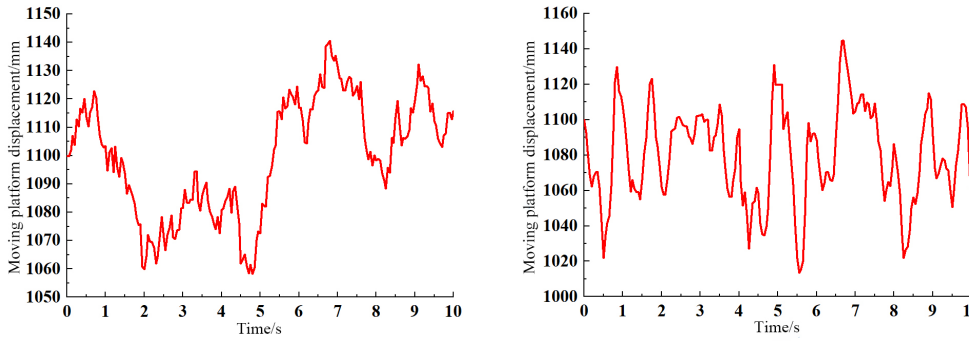

a) b)

Fig. 6. Displacement changes of moving platform: a) harmonic superposition method; b) real vehicle working condition collection

The initial moving-platform height is $H = 1100$ mm. For each of the two working conditions, the target and reproduced vertical displacements are sampled at identical times. Their root-mean-square error (RMSE) is calculated as follows:

$$RMSE = \sqrt{\frac{1}{N}\sum_{i=1}^{N}[z_t(i) - z_r(i)]^2}, \tag{23}$$

where N is the number of paired samples, i is the sample index, and $z_t(i)$ and $z_r(i)$ are the target and reproduced vertical displacements, respectively, in millimetres after subtracting the same 1100 mm reference position. The result is in millimetres. Table 6 separates the two conditions. The paired numerical histories are required to calculate the entries; the plotted images alone do not establish reportable RMSE values.

The plotted responses in Figs. 5-6 indicate qualitative tracking for both conditions. Quantitative reproduction accuracy must be evaluated from the paired time histories using Eq. (23) and reported in Table 6. In this vertical-only test, the ideal inverse-kinematics commands for symmetrically arranged cylinders may coincide; multi-axis commands are not evaluated here.

Table 6. Road-spectrum reproduction RMSE for the two simulated conditions

Working condition	Target and reproduced displacement histories	RMSE / mm
Synthetic Class E road	Paired target and simulated response, common timestamps	2.1
Measured tractor rotary tillage	Paired target and simulated response, common timestamps	1.2
Note: Replace both pending entries with values calculated from the original paired numerical time histories before submission		

7. Conclusions

A 6-UPS vehicle vibration test platform was designed and evaluated by kinematic, dynamic, structural, and control-system simulations. The principal findings are:

1) Kinematic and dynamic models describe the relationship between the six driving branches and the moving platform. Horizontal Hooke joints on the fixed platform and spherical joints on the moving platform are incorporated in the mechanical design.

2) The rated-load finite-element model predicts a maximum deformation of 1.25 mm and maximum equivalent stress of 112.64 MPa. Its first reported elastic mode is 28.403 Hz, above the 25 Hz nominal upper working frequency; joint contact behavior and loaded modal characteristics require prototype verification.

3) In the reported simulations, hybrid-tuned PID gains reduce overshoot from 15.74 % to 3.80 % and settling time from 0.34 s to 0.24 s relative to Z-N tuning. The reported maximum spatial displacement error is 0.09 mm. The simulation should be checked or rerun with the dimensionless fitness function stated in Eq. (22).

4) Synthetic Class E and measured tractor rotary-tillage displacement histories were applied in vertical-direction simulation. The figures show qualitative tracking; quantitative RMSE values for both conditions require the paired target and response histories.

The work is limited to design and simulation; a physical prototype has not yet been validated. Prototype testing will assess static strength, joint contact stress and wear, loaded modal behavior, controller timing, step response, and road-spectrum reproduction accuracy.

Acknowledgements

This research was funded by the National Natural Science Foundation of China, grant number 52302408; Key Research and Development Project of Henan Province, grant number 241111241800.

Data availability

The datasets generated during and/or analyzed during the current study are available from the corresponding author on reasonable request.

Author contributions

Huakui Chen: conceptualization, methodology, software. Xuan Jia: formal analysis, validation. Shuai Zhang: data curation, investigation, resources. Yuqing Xi: writing-original draft, writing-review and editing. Kui Liu: supervision, visualization. Yuzhuo Zhang: funding acquisition, project administration. All authors have read and agreed to the published version of the manuscript.

Conflict of interest

The authors declare that they have no conflict of interest.

References

[1] H. Liang and H. Yao, "Construction of China's automobile financial market network and its sustainability evaluation," *Frontiers in Environmental Science*, Vol. 10, p. 907311, 2022, https://doi.org/10.3389/fenvs.2022.907311

[2] S. Zhang, R. Li, D. Lu, L. Xu, and W. Xu, "Multi-objective optimization design of assembled wheel lightweight based on implicit parametric method and modified NSGA-II," *IEEE Access*, Vol. 11, pp. 71387–71406, May 2023, https://doi.org/10.1109/access.2023.3279277

[3] D. J. Park, M. G. Choi, J. T. Song, S. J. Ahn, and W. B. Jeong, "Attention decrease of drivers exposed to vibration from military vehicles when driving in terrain conditions," *International Journal of Industrial Ergonomics*, Vol. 72, pp. 363–371, Jul. 2019, https://doi.org/10.1016/j.ergon.2019.06.014

[4] J. Yoo, S. Lim, W. Kim, D. Kim, D. Yoon, and N.-C. Park, "Evaluation of vibrotactile sensation level for vehicle accelerator pedal vibration considering the sensitivity of the foot sole," *Journal of Mechanical Science and Technology*, Vol. 37, No. 3, pp. 1207–1221, Feb. 2023, https://doi.org/10.1007/s12206-023-0208-0

[5] X. Yuan, Y. Tang, W. Wang, and L. Zhang, "Parametric vibration analysis of a six-degree-of-freedom electro-hydraulic Stewart platform," *Shock and Vibration*, Vol. 2021, No. 1, p. 052059, 2021, https://doi.org/10.1155/2021/9994786

[6] X. Wu, K. Wang, Y. Wang, and S. Bai, "Kinematic design and analysis of a 6-DOF spatial five-Bar linkage," *Mechanism and Machine Theory*, Vol. 158, p. 104227, Dec. 2020, https://doi.org/10.1016/j.mechmachtheory.2020.104227

[7] M. Maleki Roudposhti and S. Haghzad Klidbary, "Development of a novel wheeled parallel robot with six degrees of freedom," *Arabian Journal for Science and Engineering*, Vol. 48, No. 3, pp. 2633–2651, Jun. 2022, https://doi.org/10.1007/s13369-022-06950-y

[8] D. Li, S. Hu, S. Xing, L. Zhang, T. Xie, and J. Yao, "A PD sliding mode swing suppression control method for bridge cranes with an improved reaching law," *Proceedings of the Institution of Mechanical Engineers, Part I: Journal of Systems and Control Engineering*, Vol. 239, No. 6, pp. 955–967, Jan. 2025, https://doi.org/10.1177/09596518241309126

[9] Z. Zhou, H. Qu, X. Li, B. Hu, and S. Guo, "Error sensitivity analysis of a 1T2R kinematically redundant parallel mechanism with closed-loop chain," *Journal of Mechanical Design*, Vol. 147, No. 5, p. 053301, May 2025, https://doi.org/10.1115/1.4066747

[10] J. Qu et al., "Nonlinear modeling and torsional vibration analysis of heavy-duty vehicle powertrain system during acceleration," *Advances in Mechanical Engineering*, Vol. 16, No. 7, p. 16878132241263936, Jul. 2024, https://doi.org/10.1177/16878132241263936

[11] W. Szczypinski-Sala, A. Kot, and M. Hankus, "The evaluation of vehicle vibrations excited with a test plate during technical inspection of vehicle suspension," *Applied Sciences*, Vol. 13, No. 1, p. 11, Dec. 2022, https://doi.org/10.3390/app13010011

[12] L. Konieczny, P. Fabis, J. Matijošius, K. Duda, P. Deuszkiewicz, and A. Kilikevičius, "Analysis of the impact of vibrations on the driver of a motor vehicle," *Applied Sciences*, Vol. 15, No. 10, p. 5510, May 2025, https://doi.org/10.3390/app15105510

[13] B. Liao, Y. Xie, D. Zhou, Y. Zhu, and H. Wei, "Vibration transfer analysis of a 6-DOF platform with oblique-mounted pyramid configuration and rigidly-hinged-mixed support," *Measurement Science and Technology*, Vol. 36, No. 5, p. 055902, May 2025, https://doi.org/10.1088/1361-6501/adcad6

[14] G. Zhan et al., "A docking mechanism based on a Stewart platform and its tracking control based on information fusion algorithm," *Sensors*, Vol. 22, No. 3, p. 770, Jan. 2022, https://doi.org/10.3390/s22030770

[15] Y.-S. Kim, H. Shi, N. Dagalakis, J. Marvel, and G. Cheok, "Design of a six-DOF motion tracking system based on a Stewart platform and ball-and-socket joints," *Mechanism and Machine Theory*, Vol. 133, pp. 84–94, Nov. 2018, https://doi.org/10.1016/j.mechmachtheory.2018.10.021

[16] W. Wang, N. Wang, and X. Wu, "Kinematics and dynamics analysis of a six-degree of freedom parallel manipulator," *International Journal of Advanced Robotic Systems*, Vol. 19, No. 5, p. 172988062211320, Sep. 2022, https://doi.org/10.1177/17298806221132077

[17] X. Huang, L. Kong, and G. Dong, "Modeling and compensation of motion errors for 6-DOF robotic manipulators," *Applied Sciences*, Vol. 11, No. 21, p. 10100, Oct. 2021, https://doi.org/10.3390/app112110100

[18] B. Li, S. Guo, X. Mao, B. Cai, and B. Wang, "Design and simulation analysis of 6-DOF electric platform," *IOP Conference Series: Materials Science and Engineering*, Vol. 563, No. 5, p. 052059, 2019, https://doi.org/10.1088/1757-899x/563/5/052059

[19] D.-A. Pham and D.-T. Nguyen, "Auto-tuning parameters of motion cueing algorithms for high performance driving simulator based on Kuka Robocoaster," *Science Progress*, Vol. 105, No. 2, p. 00368504221104333, May 2022, https://doi.org/10.1177/00368504221104333

[20] V. S. Arconada, J. García-Barruetabeña, and R. Haas, "Validation of a ride comfort simulation strategy on an electric Stewart platform for real road driving applications," *Journal of Low Frequency Noise, Vibration and Active Control*, Vol. 42, No. 1, pp. 368–391, Sep. 2022, https://doi.org/10.1177/14613484221122109

[21] Y. Zheng, X. Zhang, Y. Luo, S. Xie, and Y. Zhang, "Harnessing the compressed-spring mechanism for a six-degrees-of-freedom quasi-zero-stiffness vibration isolation platform," *Journal of Vibration and Control*, Vol. 27, No. 15-16, pp. 1793–1805, Aug. 2020, https://doi.org/10.1177/1077546320948399

[22] H. Song, X. Chen, S. Zhang, and L. Xu, "Multi-objective optimization design of 6-UPS parallel mechanism based on Taguchi method and entropy-weighted gray relational analysis," *Applied Sciences*, Vol. 12, No. 12, p. 5836, Jun. 2022, https://doi.org/10.3390/app12125836

[23] Y. Liu, H. Wu, Y. Yang, S. Zou, X. Zhang, and Y. Wang, "Symmetrical workspace of 6-UPS parallel robot using tilt and torsion angles," *Mathematical Problems in Engineering*, Vol. 2018, pp. 1–10, Jun. 2018, https://doi.org/10.1155/2018/6412030

[24] Y. Zhang, C. Cai, Z. Liu, and D. Zheng, "Space-to-plane decoupling method for six-degree-of-freedom motion measurements," *Measurement Science and Technology*, Vol. 32, No. 12, p. 125005, Dec. 2021, https://doi.org/10.1088/1361-6501/ac17cc

[25] M. Liu et al., "Kinematics model optimization algorithm for six degrees of freedom parallel platform," *Applied Sciences*, Vol. 13, No. 5, p. 3082, Feb. 2023, https://doi.org/10.3390/app13053082

[26] S.-M. Lee and H. Son, "Improvement of design and motion control for motion platform based on spherical wheels," *IEEE/ASME Transactions on Mechatronics*, Vol. 24, No. 5, pp. 2427–2433, Aug. 2019, https://doi.org/10.1109/tmech.2019.2933553

[27] X. Jing and C. Li, "Dynamic modeling and solution of 6-DOF parallel mechanism," *IEEE Access*, Vol. 10, pp. 33695–33703, Mar. 2022, https://doi.org/10.1109/access.2022.3162367



Huakui Chen received the M.Sc. degree from China. He is currently a Lecturer at the School of Automotive and Rail Transit, Luoyang Polytechnic, Luoyang, China. His research interests include vehicle electronic control technology, vehicle fault diagnosis, and parallel-mechanism vibration test platforms.



Xuan Jia is currently pursuing the M.Sc. degree in vehicle engineering at the School of Vehicle and Traffic Engineering, Henan University of Science and Technology, Luoyang, China. His research interests focus on kinematics and dynamics of parallel mechanisms and vibration-platform control.



Shang Zhang received the B.S. and M.S. degrees in vehicle engineering from the Henan University of Science and Technology, Luoyang, China, in 2011 and 2014, respectively, and the Ph.D. degree in vehicle engineering from Jilin University, Jilin, China, in 2018. Since 2018, he has been a Lecturer and now an Associate Professor with the College of Vehicle and Traffic Engineering, Henan University of Science and Technology. His research interests include research and innovation of automobile structure design theory and key technology.



Yuqing Xi received the M.Sc. degree from China. She is currently a Lecturer at Luoyang Vocational College of Science and Technology, Luoyang, China. Her research interests cover vehicle electrical control, test-system simulation and data-processing technology.



Kui Liu received the bachelor's degree in automotive service engineering from Nanyang Institute of Technology. He received the M.Sc. degree in vehicle engineering from Henan University of Science and Technology, Luoyang, China, in 2023. He is currently a Senior Engineer at China YITUO Group Co., Ltd., Luoyang, China. His research interests include structural lightweight design, off-road vehicle vibration testing and performance evaluation.



Yuzhuo Zhang received the B.S. degree in automation and the Ph.D. degree in traffic information engineering and control from Beijing Jiaotong University, Beijing, China, in 2012 and 2020, respectively. He is currently a Lecturer at the School of Vehicle and Traffic Engineering, Henan University of Science and Technology, Luoyang, China. His research interests include intelligent optimization algorithms, fault diagnosis and vehicle vibration test technology.